Chemical Geology 691 (2025) 122857

Contents lists available at ScienceDirect

Chemical Geology

journal homepage: www.elsevier.com/locate/chemgeo

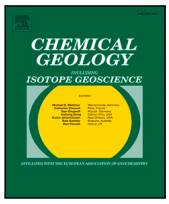

Research paper

Precession-driven variations in phosphorus cycling facilitated Earth's oxygenation in the early Proterozoic

Wytze K. Lenstra [a,b,*], Margriet L. Lantink [b,c], Rick Hennekam [d], Paul R.D. Mason [b], Gert-Jan Reichart [b,d], Frederik J. Hilgen [b], Caroline P. Slomp [a,b]

[a] Department of Microbiology, Radboud Institute for Biological and Environmental Sciences, Radboud University Nijmegen, 6525 AJ Nijmegen, The Netherlands
[b] Department of Earth Sciences, Utrecht University, 3584 CB Utrecht, The Netherlands
[c] Department of Geoscience, University of Wisconsin-Madison, WI 53706, USA
[d] Department of Ocean Systems, NIOZ, Netherlands Institute for Sea Research and Utrecht University, 1797 NZ Texel, The Netherlands

ARTICLE INFO

Communicated by Christian France-Lanord

Keywords:
Phosphorus
Great oxidation event
Reactive transport modeling
Banded iron formations

ABSTRACT

Oxygenic photosynthesis in the ocean of the early Proterozoic may have been limited by the nutrient phosphorus. If so, precession-driven variations in riverine phosphorus input may have enhanced oxygenic photosynthesis and thereby contributed to the rise of atmospheric oxygen. Here, we combine geochemical analyses of 2.46-billion-year-old deposits of the Joffre Member of the Brockman Iron Formation (Australia) and results of a reactive transport model to reconstruct pathways of organic matter degradation and phosphorus cycling in oceanic sediments over a precession cycle. Our results support a conceptual model in which increased phosphorus availability during precession maxima at southern paleolatitudes drove net oxygen production by inducing increased reductant burial in the sediment (mainly as pyrite, vivianite and magnetite). During precession minima, legacy benthic release of methane may have enhanced photolysis of atmospheric methane, thereby allowing for additional net oxygen production. Hence, precession-driven variations in coupled carbon–phosphorus–oxygen cycling may have acted as an accelerator towards the Great Oxidation Event.

1. Introduction

The emergence of oxygen in the Earth's atmosphere during the Great Oxidation Event (GOE), ca. 2.4 to 2.2 billion years ago (Poulton et al., 2021), dramatically altered global biogeochemical cycling and the evolution of life (Canfield et al., 2006; Lyons et al., 2014; Cohen and Kodner, 2022). Importantly, microorganisms capable of oxygenic photosynthesis possibly evolved even as early as ca. 3 billion years ago (Fournier et al., 2021), i.e. well before the GOE. This implies low rates of initial oxygen production and/or highly efficient removal of oxygen by reductants that were abundantly present at the Earth's surface (Catling et al., 2001; Canfield, 2005; Holland, 2006). Geochemical evidence points towards a dynamic and shifting balance between the production and removal of oxygen leading to both whiffs of oxygen in the atmosphere and oxygen oases in the ocean before the GOE (Anbar et al., 2007; Kendall et al., 2010; Ostrander et al., 2021; Wogan et al., 2022; Anbar et al., 2023). The factors controlling oxygen dynamics are debated and include limitation of oxygenic photosynthesis by the availability of phosphorus (Kipp and Stüeken, 2017; Hao et al., 2020b), other nutrients and evolutionary constraints (Crockford and Halevy, 2022).

Here, we follow the line of thought that the availability of the nutrient phosphorus limited photosynthesis in the mostly ferruginous ocean of the Archean and early Proterozoic prior to the GOE (Canfield et al., 2006; Jones et al., 2015; Reinhard et al., 2017). Under phosphorus limitation, anoxic photoferrotrophs will have been favored over oxygenic cyanobacteria because of the adaption of the former to lower light conditions and hence their ability to outcompete the latter for phosphorus supplied through upwelling (Canfield et al., 2006; Jones et al., 2015). The oxidation of dissolved Fe^{2+} that is associated with photoferrotrophy, in turn, is thought to have led to formation of iron oxide-rich, organic matter-lean deposits, so-called Banded Iron Formations (BIFs) (Konhauser et al., 2002; Kappler et al., 2005). Microaerophilic Fe-oxidizing microorganism and/or the reaction of Fe^{2+} with free O_2 might also have contributed to the formation of Fe oxide-rich sediments (Chan et al., 2016). Scavenging of phosphorus by the iron oxides (Bjerrum and Canfield, 2002) and/or a dearth of oxidizing

* Corresponding author at: Department of Microbiology, Radboud Institute for Biological and Environmental Sciences, Radboud University Nijmegen, 6525 AJ Nijmegen, The Netherlands.
E-mail address: wytze.lenstra@ru.nl (W.K. Lenstra).

https://doi.org/10.1016/j.chemgeo.2025.122857
Received 5 February 2025; Received in revised form 7 May 2025; Accepted 13 May 2025
Available online 6 June 2025

power (Kipp and Stüeken, 2017) may have limited recycling of phosphorus, thereby maintaining low dissolved phosphate concentrations and, consequently low rates of oxygenic photosynthesis in the ocean. In such an oceanic setting, an increased weathering supply of phosphorus (Hao et al., 2020a) and/or increased benthic recycling (Alcott et al., 2022) would lead to a higher rate of oxygenic photosynthesis, an increased flux of organic matter to the seafloor and the potential formation of oxygen oases.

Recently, Lantink et al. (2023) explained cyclic enrichments in sedimentary iron, sulfur and phosphorus in 2.46 billion year-old BIFs by precession-driven variations in riverine phosphorus supply. Using a reactive transport model for sediment diagenesis, the authors showed that the distinct pattern in iron and sulfur enrichments was consistent with a model scenario with periodic variations in water column oxygenation and iron oxide and organic matter input to the sediment (Lantink et al., 2023). Concomitant variations in oxygenic photosynthesis were proposed to be driven by precession-induced changes in monsoonal intensity and associated variations in runoff and phosphorus delivery from land (see supplements and Lantink et al. (2023) for a detailed discussion). However, the sedimentary phosphorus cycle was not included in this model.

Importantly, oxygen can only accumulate in the ocean and atmosphere if either the organic matter itself or the reduced products of its anaerobic degradation are retained in the sediment (Canfield, 2005). Prior to the GOE, sulfate concentrations in the ocean were low (<200 μmol L^{-1}; Habicht et al. (2002), Zhelezinskaia et al. (2014), Crowe et al. (2014)). This implies that iron oxide reduction and methanogenesis would have accounted for a major proportion of the anaerobic degradation of organic matter (Crowe et al., 2011; Thompson et al., 2019). Hence, the fate of the reduced products of these processes, namely Fe^{2+} and methane, are of key relevance to the timeline and rate of the emergence of oxygen. Part of the methane might have been removed in the sediment through anaerobic oxidation of methane coupled to Fe oxide reduction (Fe-AOM) (Beal et al., 2009; Egger et al., 2015). Dissolved Fe^{2+} could have been sequestered in a range of minerals, including pyrite, vivianite and magnetite. How the balance between oxygen production and the benthic recycling of reductants varied during the early Proterozoic and how this impacted the eventual oxygenation of the atmosphere is largely unknown.

In this study, we build upon the recent modeling work of Lantink et al. (2023) by including the sedimentary cycle of the nutrient phosphorus in the reactive transport model. Subsequently, we use the model to describe the redox cycles as recorded in the sedimentary record in the BIFs of the Joffre Member of the Brockmann Iron Formation. This 2.46 billion year-old BIF is part of the upper Neoarchean to lower Proterozoic Hamersley Group in Western Australia. With this transient model, we first test whether the scenario of increased phosphorus input as a driver of increased oxygenic photosynthesis is in line with the geochemical record. We then use the model to quantify the pathways of organic matter degradation in the sediment and assess the fate of the reductants produced. These model results allow us to assess the role of key pathways of oxygen production prior to the GOE. Importantly, this information cannot be deduced from the sedimentary record without such a model. Due to the cyclostratigraphic framework associated with this model we are able to determine these processes in unprecedented detail. We conclude that periods of astronomically controlled input of phosphorus may have contributed to the eventual oxygenation of Earth's atmosphere by enhancing oxygenic photosynthesis and the production of organic matter that ultimately promoted the burial of reductants and, potentially, rates of photolysis of methane in the atmosphere. Taken together, the results of this study suggest that, by modulating the phosphorus supply, astronomically-driven climate change may have acted as an important control on the pace of the oxygenation of our planet.

2. Methods

2.1. Reactive transport model

A detailed description of the model is given in the supplements. Briefly, the model describes the mass balance of 6 dissolved and 11 particulate species (Table S.1). The model domain consists of a one-dimensional grid of 1000 evenly distributed cells that captures the interval from the sediment–water interface to a depth of 100 cm. All chemical species are subject to biogeochemical reactions (Table S.2). Solids and solutes are transported by sediment accumulation. Solutes are additionally transported by molecular diffusion (Wang and Cappellen, 1996; Boudreau, 1997).

2.2. Boundary conditions and the transient scenario

Bottom water concentrations of solutes are based on the range known from the literature while fluxes of solids towards the sediment–water interface are constrained by total elemental contents of iron, sulfur and phosphorus with depth in the sediment as determined by calibrated XRF (Lantink et al. (2023); Table S.6). The sedimentation rate of 20 cm kyr^{-1} was based on U/Pb dating, assuming a porosity of 0.95 (vol/vol) at the sediment–water interface (Lantink et al. (2023); Table S.4). For a detailed description of the U-Pb dating, cyclostratigraphic analysis and interpretation see Lantink et al. (2022).

The model was first run to steady state for 17 kyrs. This was followed by the implementation of a transient scenario of 35 kyrs to capture key aspects of two precessional cycles. The transient scenario follows our conceptual model in which phosphorus input is low during precession minima and increases during precession maxima, leading to alternating periods of anoxygenic photoferrotrophy and oxygenic photosynthesis.

In this transient scenario, the bottom water concentration of Fe^{2+} and the input flux of organic matter, iron oxides and particulate phosphorus at the sediment–water interface were varied with time (Fig. 1). Importantly, these boundary conditions were constrained by the solid phase data and process knowledge from the literature, i.e. while values were chosen that gave the best fit to the sediment profiles, the degrees of freedom were limited by the large number of model components, the specific parameter ranges expected for the depositional environment, and the reaction kinetics and parameters known from the literature, as upon the application of these types of models in modern sediments (Cappellen and Wang, 1996). Below, we describe the transient scenario that we used to test our conceptual model. We focus specifically on a description of the changes from a precession minimum to a precession maximum (Fig. 1).

In our model we assume a low organic matter deposition during precession minima (0.61 mmol m^{-2} yr^{-1}), and a strong increase to ca. 43 mmol m^{-2} yr^{-1} during precession maxima (Table S.6 and Fig. 1A). Here the maximum deposition of organic matter is constrained by the sedimentation rate (Lantink et al., 2023) and the rate of SO_4^{2-} reduction and formation of H_2S and Fe sulfides that, in turn, are constrained by the sedimentary record. We note that our scenario is in accordance with the assumption that primary productivity and subsequent deposition of organic matter during the late Archean - early Proterozoic was low (Hao et al. (2020b) and references therein).

During precession minima the bottom water Fe^{2+} concentration was 30 μmol L^{-1} (Konhauser et al., 2017) and the deposition of Fe oxides was high (i.e. 152 mmol m^{-2} yr^{-1} and Figs. 1B and C). During the onset period of oxygenic photosynthesis, the bottom water Fe^{2+} in the model decreased to 0, while rates of Fe oxide deposition increased. This is in line with what would be expected upon the emergence of oxygen in seawater (Millero et al., 1987). In the model we assume that the concentration of bottom water Fe^{2+} then remained low and the deposition of Fe oxides decreased to ca. 4.5 mmol m^{-2} yr^{-1}, reflecting the lower deposition of Fe oxides because of the limited formation of

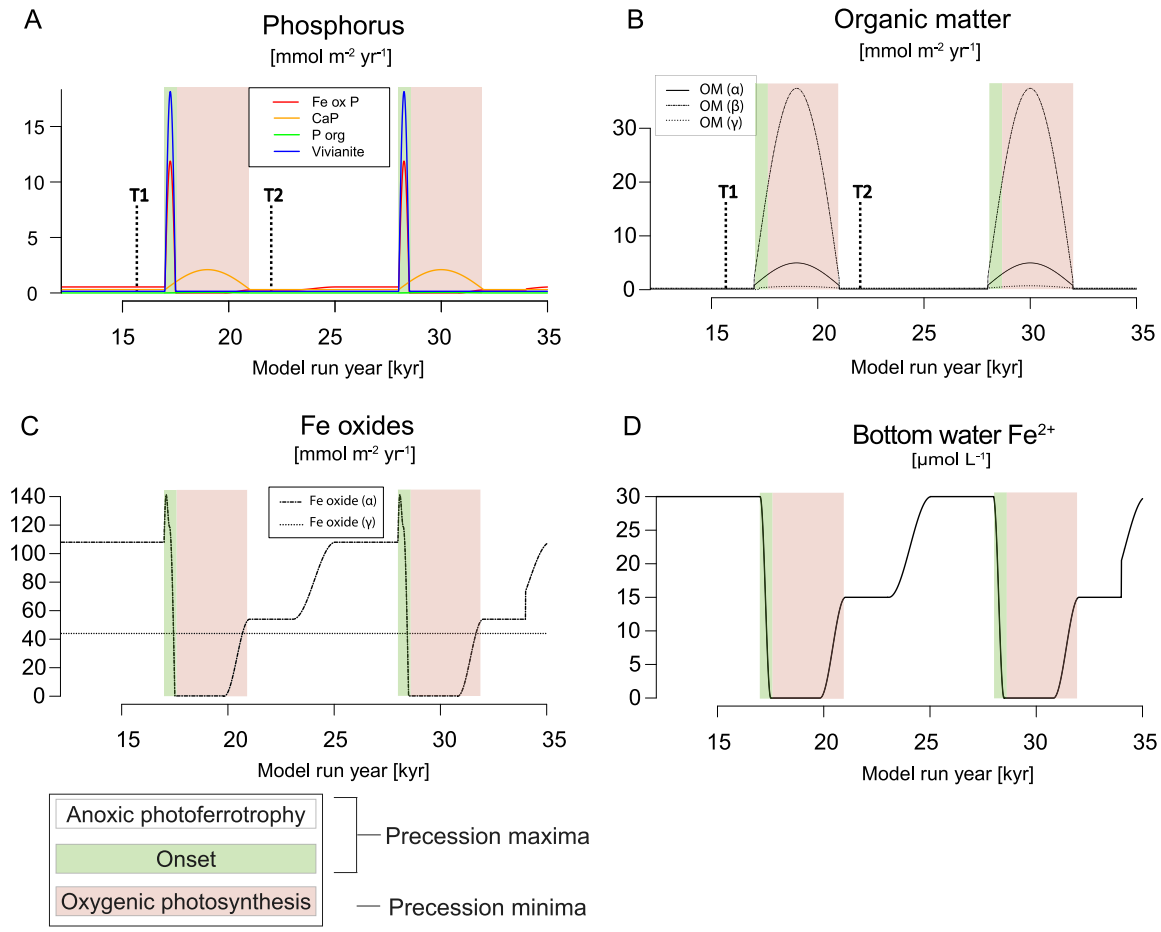

Fig. 1. Transient fluxes and bottom water concentration at the sediment water interface; (**A**) different forms of phosphorus deposition; (**B**) different forms of organic matter deposition; (**C**) different forms of Fe oxide deposition and (**D**) bottom water Fe^{2+}. T1 and T2 refer to 16 kyr and 22 kyr, respectively. Data of all time dependent fluxes and bottom water Fe^{2+} are available as data in the supplementary data files.

Fe oxides in the water column. At the end of the period of oxygenic photosynthesis, the bottom water Fe^{2+} concentrations and Fe oxide deposition steadily increased again, in line with the increase of the dissolved Fe inventory that is expected when the water column is anoxic.

In the model, we assume that the rate of deposition of P at the seafloor was low during precession minima, in accordance with the low P content in the sediment (Figs. 1D and 2). During these periods, the rate of deposition of Fe oxides was high and we therefore assume that most P that was deposited was bound to Fe oxides or consisted of detrital apatite (CaP). The speciation of P in sediments or rocks can help with unraveling the mechanisms controlling P deposition on the seafloor and subsequent diagenesis (Ruttenberg, 2013). However, when studying BIFs, post-depositional metamorphism excludes the use of mineral analyses and P speciation to deduce the original sediment P forms. For example, sedimentary vivianite is thought to have reacted irreversibly with calcite to form apatite (Hao et al., 2020b), which makes it impossible to quantify the importance of vivianite in the burial of P. Therefore, at this point, we can only reconstruct the P speciation in the model using constraints from the other elemental cycles.

During precession maxima, we assume a strong increase in the input of riverine HPO_4^{2-}. Since dissolved Fe was abundantly present in the water column we assume that this increase in HPO_4^{2-} input led to the formation and deposition of vivianite (Derry, 2015) and enhanced deposition of P bound to Fe oxides. Together with HPO_4^{2-} also the input of CaP increased, which is in line with the key riverine P sources recently presented (Hao et al., 2020a). In the periods of oxygenic photosynthesis, the bottom water Fe^{2+} and Fe oxide deposition was low, resulting in limited deposition of vivianite and P bound to Fe oxides. At the end of the period of oxygenic photosynthesis, the deposition of P bound to Fe oxides increased again, which is in accordance with an increasing oceanic dissolved Fe inventory and the presence of anoxic photoferrotrophs.

2.3. Sensitivity analysis

A model sensitivity analysis was performed to investigate the effects of changes in two key processes that impact net oxygen production: (1) reductant burial and (2) benthic methane release. These processes are expected to be especially sensitive to the bottom water SO_4^{2-} concentration (Canfield, 2005) and the rate of Fe-oxide driven AOM (Konhauser et al., 2005). Here, we varied the bottom water SO_4^{2-} concentrations over a range from 2.5–500 µmol L^{-1}. The impact of variations in Fe oxide driven AOM on the oxidation and benthic release of methane was investigated by varying the rate constant, k_8 (Table S.5), over two orders of magnitude (i.e. 2.1–210 $mmol^{-1}$ L yr^{-1}). During all model runs in the sensitivity analysis, the transient baseline scenario was used (Fig. 1) and only one factor was varied per run.

3. Results and discussion

3.1. Phosphorus limitation and oxygenic photosynthesis

The lower Proterozoic deposits of the Joffre Member are characterized by distinct cyclic alternations in potassium, iron, sulfur and

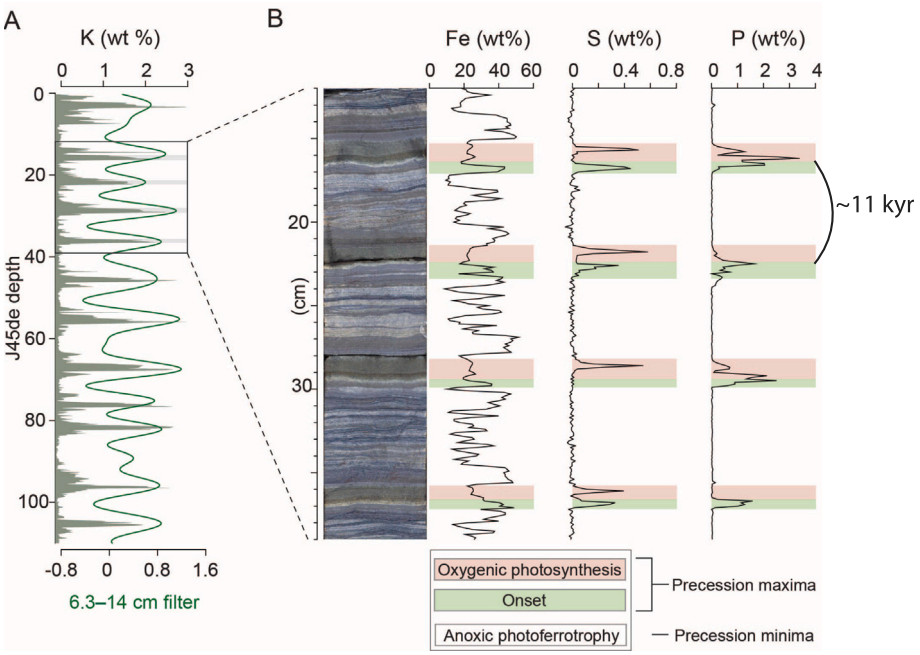

Fig. 2. Detail of four Knox cyclothem alternations (cm to dm-scale rhythmic lithological alternations; (Trendall and Blockley, 1968)) in section J45de from depths of 289.05 to 290.26 m in core DD98 from the Joffre Member of the Brockman Iron Formation (modified from Lantink et al. (2023)). (**A**) Regular small-scale alternations reflected in the K record (wt%) of section J45de and corresponding bandpass filtered curve (thick green line). (**B**) The lithology is shown on the left while Fe, S and P (wt%) records are shown on the right. For the geological and stratigraphic background, we refer to Lantink et al. (2023). Precession minima are associated with low K, S and P input and anoxic photoferrotrophy (white), precession maxima are associated with oxygenic photosynthesis (pink). The 11 kyr precessional cycle indicated in the figure corresponds to the precessional cycle implemented in the model (Fig. 1).

phosphorus contents (Fig. 2), which have been linked to Earth's precessional cycle (ca. 11 kyrs; Lantink et al. (2023)). While iron oxide-rich and phosphorus- and sulfur-poor deposits were formed during precession minima at inferred southern paleolatitudes and periods of low monsoonal intensity (see supplements and Lantink et al. (2023)), the records associated with precession maxima and periods of enhanced monsoonal intensity show a more complex diagenetic pattern associated with elevated organic matter input (Lantink et al., 2023). Here, we will discuss the key aspects relevant to the phosphorus cycle and the ultimate impact on oxygenic photosynthesis.

The low phosphorus contents in the sediments during periods of low monsoonal intensity and relatively low terrigenous input (Lantink et al., 2023), suggest a marine environment limited by phosphorus possibly because of low riverine input (Lantink et al. (2023); Figs. 2, 3A and 3C). Additionally, variations in upwelling and benthic recycling of phosphorus on the precession scale could have amplified the rhythmic alterations in the phosphorus records. Because of the anoxic and weakly reducing atmosphere with high levels of carbon dioxide, riverine phosphorus loads are expected to have carried detrital CaP and dissolved phosphate to the ocean (Hao et al., 2020a). Only the latter will have been bioavailable; the apatite will have been buried without alteration (Hao et al., 2020b). The low availability of phosphate in the ocean is thought to have enabled iron-dependent anoxygenic photosynthesis (anoxic photoferrotrophy) and hence the production of iron oxides in the water column (Kappler et al., 2005; Thompson et al., 2019). Scavenging of phosphorus from the water column by sorption to iron oxides and by vivianite formation and subsequent burial of the iron minerals in the sediment will have limited recycling of the phosphate (Derry, 2015; Halevy et al., 2017; Hao et al., 2020a). In our conceptual and quantitative model scenario for precession minima (Fig. 3A and 3C), we assume that P bound to Fe oxides and apatite were responsible for the majority of the phosphorus reaching the seafloor (in the model: ~64% and ~35%, respectively), with vivianite and organic P accounting for the remainder (<1%; Fig. 1). In the model, most phosphate released from organic matter in the sediment is readsorbed onto Fe oxides. Phosphorus is mainly buried as P bound to Fe oxides and CaP and remains below 30 μmol g^{-1} (Fig. S.1).

The succeeding period of enhanced monsoonal intensity can be separated into an onset phase and a phase of maximum precession (i.e. maximum monsoonal intensity Lantink et al. (2023); Fig. 2). During the onset, sedimentary phosphorus contents increased strongly to values that sometimes exceed 3 wt% (Fig. 2). While the P content remains under the threshold for phosphorites (i.e. 10–20 wt%; Filippelli (2011)), the total phosphorus contents are much higher than those reported for contemporaneous shales before the GOE (<0.37 wt%; Reinhard et al., 2017). During the late Archean, weathering fluxes of P likely strongly increased and a major increase in P flux to the ocean is suggested to have occurred close to the Archean-Proterozoic boundary due to an increased continental emergence (Hao et al., 2020a). Our data are in accordance with this prior research and suggest that P inputs varied in response to variations in monsoonal intensity. In this interpretation, the high P contents and associated enhanced terrigenous input (Lantink et al., 2023) are indicators of increased riverine input of P to the ocean. The sedimentary enrichment in P may have been amplified by redox-dependent deposition and diagenesis of P-bearing particles (Filippelli, 2011).

The increased input of dissolved phosphate is expected to have led to higher rates of primary productivity by promoting oxygenic photosynthesis at the expense of anoxic photoferrotrophy. Increased phosphorus availability in an anoxic iron-rich ocean can shift the ratio of dissolved Fe^{2+} and phosphate to below the value of 424 required by photoferrotrophs, which is based on a C:P ratio of 106:1 and a Fe:C ratio of 4:1, implying a Fe:C:P ratio of 424:106:1 (Canfield et al., 2006; Jones et al., 2015), thereby creating a niche for oxygenic cyanobacteria. The associated production of oxygen is not expected to have led to oxygenation of the water column during this phase, however, because of the abundant presence of dissolved Fe^{2+}, which could readily react with the oxygen. Indeed, during every onset, enhanced burial of iron is observed, with a subsequent decrease towards the end of the onset phase (green area in Fig. 2), which we attribute to loss of most dissolved Fe^{2+} from the water column (Fig. 3). During this phase, nearly

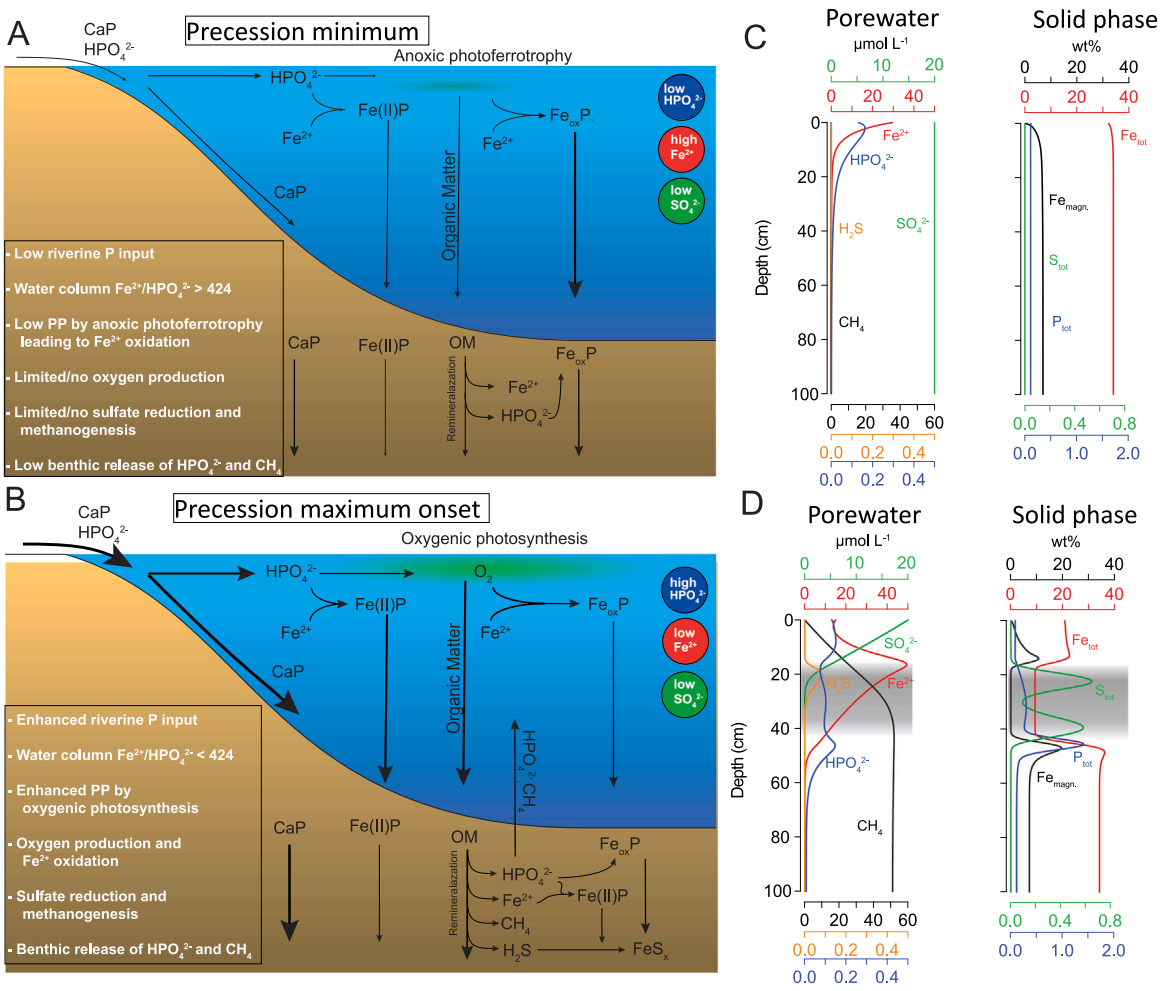

Fig. 3. Conceptual model of marine phosphorus cycling (**A**) during precession minima, with low riverine input of phosphorus, high dissolved Fe^{2+} concentrations and anoxic photoferrotrophy in the water column; (**B**) during precession maxima, with high riverine input of phosphorus, low dissolved Fe^{2+} concentrations and oxygenic photosynthesis in the water column. Model calculated profiles of (**C, D**) pore water Fe^{2+}, SO_4^{2-}, H_2S, methane and HPO_4^{2-} and solid phase total Fe (Fe_{tot}), magnetite ($Fe_{magn.}$), total sulfur (S(tot) and total phosphorus (P_{tot}), corresponding with the scenarios of (A) and (B), respectively. The timing relevant to the profiles is indicated in Fig. 1 (T = 1 and T = 2, respectively). Shading in figure D indicates the period of enhanced organic matter deposition on the seafloor during precession maxima. The speciation of P_{tot} in D is presented in Fig. S.1.

all bioavailable phosphate is expected to have been removed either with iron oxides or through rapid precipitation of vivianite (Derry, 2015). Hence the flux to the sediment of both phosphorus forms would initially have been enhanced because of the high dissolved phosphate and dissolved Fe^{2+} availability. The flux of apatite and phosphorus in organic matter will likely also have been elevated (Figs. 1 and 2). This is reflected in the burial of phosphorus in the model. During the onset period, P is mainly buried in the form of vivianite and as P bound to Fe oxides. After this initial peak of P deposition P is predominantly buried as CaP with a minor contribution of organic P (Fig. S.1).

During the subsequent precession maximum, when dissolved Fe concentrations were low and the availability of P was high, most productivity would have taken place through oxygenic photosynthesis (Figs. 3B and 3D) leading to an enhanced flux of organic matter to the sediment, a much lower Fe oxide flux (Fig. 1) and a greater role for sulfate reduction in organic matter degradation. As discussed in detail in Lantink et al. (2023) the distinct sulfur (pyrite) enrichment in the sediment of the onset phase (Figs. 2 and 3) is a diagenetic feature that is a consequence of elevated rates of sulfate reduction following the decline in water column dissolved Fe^{2+} and iron oxide deposition. The near zero dissolved Fe^{2+} concentrations in the water column point towards oxygenation of the water column (Lantink et al., 2023). We note that, in the model reconstructions of the iron and sulfur records reproduced (here Lantink et al. (2023) Fig. 3D), bottom water sulfate concentrations are only 20 μmol L^{-1}, in line with previous work (Crowe et al., 2014).

After the initial phase of enhanced Fe oxide bound P deposition (Fig. 1A), organic matter is assumed to have been the dominant source of reactive phosphorus to the sediment, with only a minor contribution from P bound to Fe oxides. In our model scenario, we assume that most P is buried as non-reactive riverine derived CaP (Hao et al., 2020a; Walton et al., 2023) with a minor contribution of authigenic CaP. The rate of deposition of Fe oxide bound P and vivianite is expected to be very low because of the near zero concentrations of Fe^{2+} in the water column (1, 3B and 3D). Therefore most P burial during the period of oxygenic photosynthesis is in the form of CaP (Fig. S.1). The lower rates of deposition of iron oxides and enhanced role for sulfate reduction could have enhanced the benthic recycling of phosphorus (Kipp and Stüeken, 2017), possibly sustaining primary productivity upon the gradual decline of riverine phosphorus input. During the successive precession minima, sediments again became sulfur- and phosphorus-poor and iron oxide-rich, indicating a return to a phosphorus-limited ocean with anoxic photoferrotrophy as the dominant pathway of organic matter production. Taken together, our work suggests that increased phosphorus input during precession maxima likely enhanced rates of primary productivity through oxygenic photosynthesis, thereby allowing oxygenation of the water column.

3.2. Pathways of organic matter degradation in the sediment and release of methane

The oscillations in the availability of phosphorus in the water column drive periods of enhanced primary productivity (i.e. organic matter production). Part of the produced organic matter is deposited on the seafloor where it impacts the degradation pathways of organic matter in the sediment and the release of reductants such as dissolved iron and methane. In anoxic photoferrotrophy, the formation of iron oxides and organic matter is directly coupled through an iron oxide to organic carbon ratio of 4 to 1 (Widdel et al., 1993). If the organic carbon and iron oxides reach the sediment together, iron oxide reduction is expected to be the dominant pathway of organic matter degradation. Recent work has shown, however, that the high dissolved silica concentration in the ocean might have led to a decoupling of the deposition of iron oxides and organic matter (Thompson et al., 2019). This could have allowed organic matter to be laterally transported and would explain why BIF sediments are so lean in organic matter (Thompson et al., 2019). The variations in sedimentary organic matter degradation pathways in our model as a result of the rise of oxygenic photosynthesis are discussed next.

Our model results suggest that the initial elevated rates of iron oxide deposition upon the onset of oxygenic photosynthesis led to a dominant role for iron oxides as an electron acceptor in organic matter degradation (Fig. 4A). In the next phase, when oxygenic photosynthesis was fully established, sulfate reduction and methanogenesis became the key pathways of organic matter degradation, accounting for up to 90% and 70% of all organic matter degradation, respectively. Such a key role for methanogenesis is expected when the supply of iron oxides and sulfate is low (Habicht et al., 2002). The initial role of sulfate is surprising but can be explained by a sharp gradient in sulfate near the sediment–water interface, allowing for continuous supply of sulfate from the bottom water (Fig. 3). Due to the high Fe content of the sediment nearly all H_2S that is produced from sulfate reduction is expected to be precipitated in the sediment as Fe sulfides. Therefore, we are able to precisely quantify the total rate of sulfate reduction. During burial of organic matter in the sediment, there is a gradual shift from sulfate reduction to methanogenesis as the dominant pathway of organic matter degradation. Neither sulfate nor iron oxides are quantitatively important oxidants for methane (Fig. 4). This implies that a large proportion of the methane that is produced in the sediment escapes to the overlying water. Importantly, the anaerobic degradation of the organic matter in the organic-rich layer continues upon burial in the sediment after reestablishment of anoxic photoferrotrophy and elevated iron oxide deposition. To assess whether a higher rate of iron oxide-driven anaerobic oxidation of methane would limit this methane release, we increased the rate constant for the process by two orders of magnitude. We still find substantial benthic release of methane, however (Fig. 4B and C). This suggests that the precession-driven variations in productivity associated with a paleo monsoon system (Supplements 1.1) not only impact the emergence of oxygen in surface waters but also can lead to loss of methane from the BIF sediments after reestablishment of water column anoxia.

3.3. BIFs and the oxygenation of the atmosphere

The increasing abundance of oxygen in the atmosphere at the GOE was the result of a permanent shift in the balance between the production and removal of oxygen in Earth surface environments. Oxygen will not accumulate if rates of oxygen production by oxygenic photosynthesis are equal to rates of oxygen removal through aerobic and anaerobic respiration of the organic matter and reoxidation of all reductants produced. If, however, the organic matter or associated reductants are buried (e.g. in pyrite), oxygen can accumulate (Canfield, 2005). There is also net oxygen production when H_2 escapes to space, a process that is thought to increase upon an increase in atmospheric levels of methane (Catling et al., 2001). The relative contribution of these two processes to net oxygen production (i.e. reductant burial versus H_2 escape) over time is largely unknown.

Table 1
Reductant burial during precession minima and maxima as calculated with the model and benthic methane release assuming that all methane that is released during precession maxima is oxidized (i.e. during periods of oxygenic photosynthesis).

	Precession minima mmol m^{-2} yr^{-1}	%	Precession maxima mmol m^{-2} yr^{-1}	%
Reductant burial				
Organic C burial	0.05	7	0.2	6
FeS_x burial	0	0	2.0	66
Magnetite burial	0.6	90	0.6	19
Vivianite burial	0.1	2	0.2	6
Fe carbonate burial	0.002	1	0.1	3
Total	0.75	100	3.1	100
Benthic methane release	1	–	0	–

During precession minima, oxygen production would have been negligible, since oxygenic photosynthesis was suppressed (Fig. 5). Our model results can provide quantitative constraints on net rates of oxygen production during precession maxima, however. If we assume that all the organic matter reaching the sediment was formed via oxygenic photosynthesis, the maximum potential rate of oxygen production would be ~16 mmol m^{-2} yr^{-1} (Fig. 5A; Table 1). According to the model, only a small part of this organic matter was buried, thereby contributing an oxygen production of 0.2 mmol m^{-2} yr^{-1}. Burial of pyrite contributed 2.0 mmol m^{-2} yr^{-1}. The sum of vivianite, magnetite and iron carbonate burial contributed an additional 0.9 mmol m^{-2} yr^{-1}. Hence, pyrite burial accounted for ca. 66% of net oxygen production through burial in sediments, with organic matter and a range of reduced iron minerals being responsible for the remainder. With our model we show that, in contrast to earlier conceptual models (Canfield, 2005), even in an ocean with very low sulfate concentrations, burial of pyrite can periodically be the main pathway of net oxygen production.

In our model results, benthic release of methane increased during precession maxima up to rates of 7 mmol m^{-2} yr^{-1} (Fig. 5C). Most of this methane would have been oxidized by oxygen produced in the water column through oxygenic photosynthesis. Importantly our model results indicate that the benthic release of methane likely continued during precession minima because of continued degradation of the organic matter deposited during previous precession maxima. This "legacy" benthic methane release (green areas in Fig. 5C) would have been released to a water column that was anoxic. Since the removal of methane from anoxic water columns is not as efficient (Steinsdóttir et al., 2022; Żygadłowska et al., 2024b; Venetz et al., 2024), part of this methane likely escaped to the atmosphere, where it could have contributed to the net production of oxygen upon photolysis and subsequent release of H_2 to space. The average benthic release of methane calculated with the model is 1 mmol m^{-2} yr^{-1}. This would be the maximum estimate of the flux of methane contributing to photolysis and, hence, oxygenation of the atmosphere.

In our model, pyrite is the key sink for reductants in the sediments during precession maxima, and hence is most critical to net oxygen production (Table 1). The rate of formation of Fe-sulfides, in turn, is limited by the rate of sulfate reduction. Given sufficient sedimentary iron and organic matter, sulfate concentrations will have acted as the key control on sulfate reduction, with a substantial rise in the rate of burial of Fe sulfides only being expected upon oxygenation of the atmosphere and an associated rise in sulfate concentrations (Bjerrum and Canfield, 2002). A sensitivity analysis illustrates the strong response of the rate of pyrite burial in our model to variations in bottom water sulfate concentrations (Fig. 6; supplementary section). Given the strong response of Fe sulfide formation to variations in bottom water sulfate (Fig. S.3 and the persistence of the double S peak

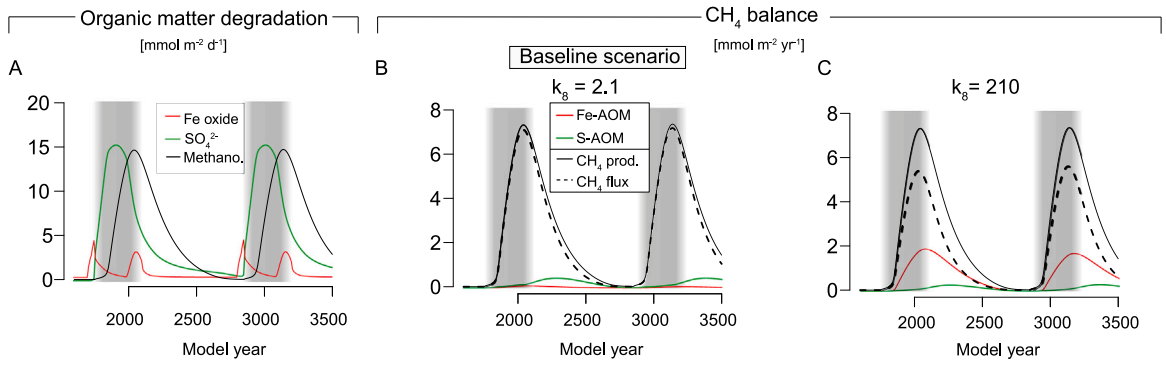

Fig. 4. (**A**) Pathways of organic matter degradation as calculated with the model; (**B**) Rates of methane production, methane removal through anaerobic oxidation coupled to reduction of Fe oxides (Fe-AOM) and sulfate (S-AOM) and the flux of methane across the sediment–water interface for the same model scenario; (**C**) The same as (B) but for a model scenario with a rate constant for methane oxidation (k_8) that is a factor 100 higher (Supplementary Table S.5). Shading indicates the timing of enhanced organic matter deposition on the seafloor during precession maxima.

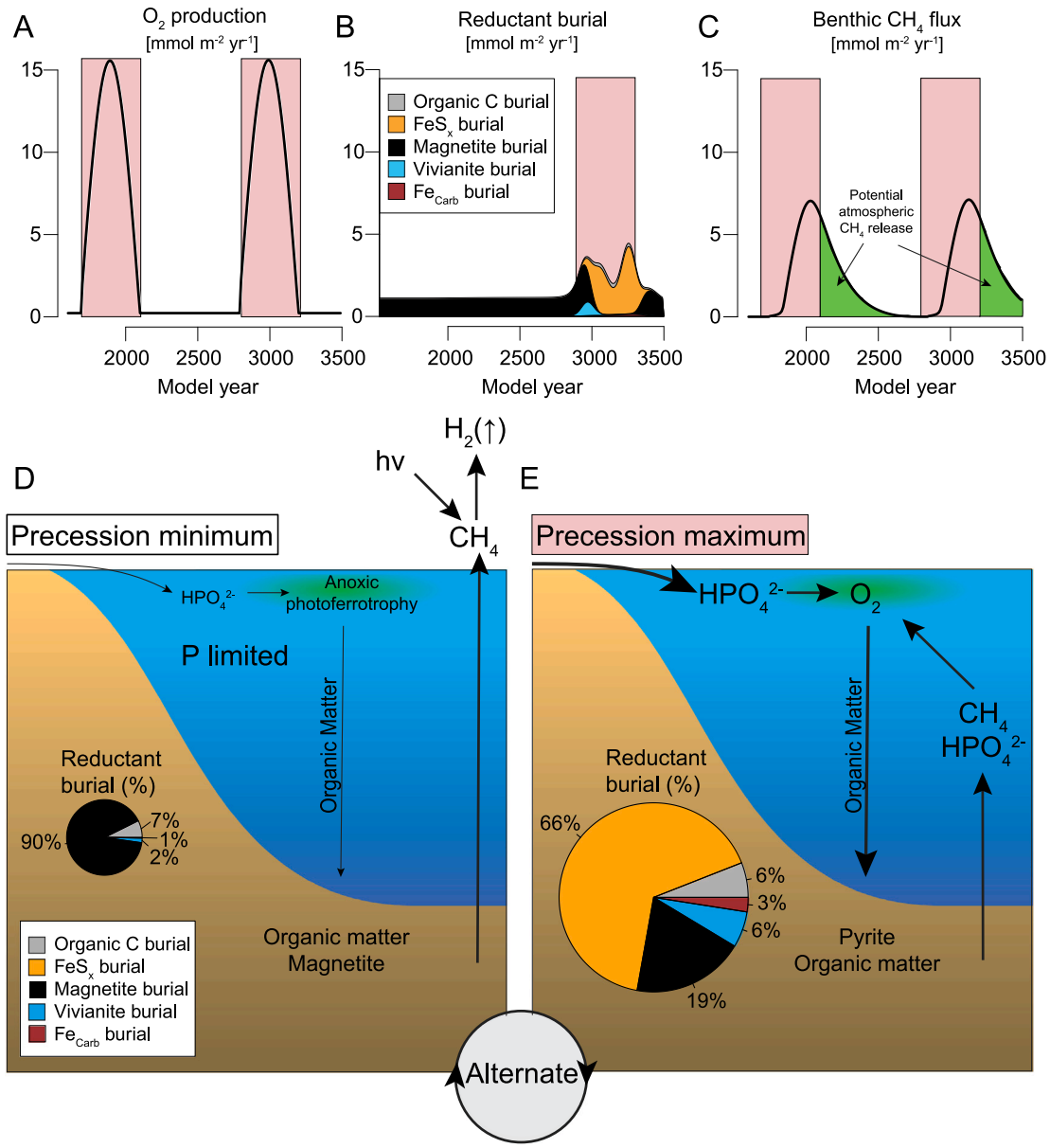

Fig. 5. (**A**) Oxygen production (mmol m^{-2} yr^{-1}) if all organic matter deposited at the sediment water interface would be buried when assuming that production takes place through oxygenic photosynthesis; (**B**) Reductant burial (mmol m^{-2} yr^{-1}, in oxygen-equivalents) at the lower boundary of the model domain at 100 cm; (**C**) Release of methane from the sediment to the water column; Pink shading: period of oxygenic photosynthesis and precession maximum; (**D**) and (**E**). Schematic overview of pathways of reduction burial and methane photolysis during precession minimum and precession maximum, respectively. The percentage of the various reductants buried in the sediment are shown in the pie chart.

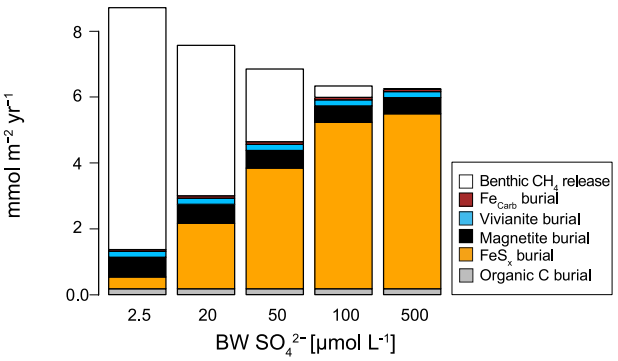

Fig. 6. The burial of reductants and benthic release of methane (in oxygen equivalents) during precession maxima as calculated with the model assuming a range of bottom water sulfate concentrations (2.5 to 500 µmol L^{-1}). Note that in the baseline model calculations the bottom water sulfate concentration is 20 µmol L^{-1}.

in our sedimentary record, large variations in bottom water sulfate concentrations are unlikely. Importantly, the rise in bottom water sulfate also impacts the production and benthic release of methane. Our results suggest that the potential contribution of photolysis of methane produced in the sediment to oxygenation of the atmosphere is lost when sulfate concentrations rise above 500 µmol L^{-1}. This sulfate concentration is even lower than a previous estimate from an Earth system model (>1000 µmol L^{-1}; Olson et al., 2016). Benthic release of methane will, however, also depend on other factors than bottom water sulfate concentrations, such as the availability of other electron acceptors and the rate of organic matter deposition (Lenstra et al., 2023; Żygadłowska et al., 2024a). This threshold can therefore vary depending on the location and geochemical context of the seafloor.

Overall, the geochemical data and model results point towards increased inputs of phosphorus to the ocean during precession maxima, as a driver of enhanced reductant burial and, possibly, escape of H_2 via photolysis of methane in the atmosphere during subsequent precession minima. Both processes likely contributed to the eventual oxygenation of the atmosphere by contributing to a gradual shift in the balance between oxidants and reductants in the ocean-atmosphere systems.

An important question that remains is: how important are astronomically-driven climatic changes for the oxygenation of the Earth? In our conceptual model, the increased availability of P during precession maxima allowed the threshold for oxygenic photosynthesis to be exceeded. As a consequence, the oceanic reservoir of reduced species decreased, paving the way for the shift in oxygen sources and sinks that ultimately allowed oxygen to accumulate in the atmosphere. Without these pulses of P, this shift may have occurred at a much later date. Hence, the astronomically-driven climatic changes and related P inputs may have accelerated Earth's oxygenation.

CRediT authorship contribution statement

Wytze K. Lenstra: Writing – review & editing, Writing – original draft, Visualization, Methodology, Investigation, Conceptualization. **Margriet L. Lantink:** Writing – review & editing, Investigation, Conceptualization. **Rick Hennekam:** Writing – review & editing. **Paul R.D. Mason:** Writing – review & editing. **Gert-Jan Reichart:** Writing – review & editing. **Frederik J. Hilgen:** Writing – review & editing, Investigation, Conceptualization. **Caroline P. Slomp:** Writing – review & editing, Writing – original draft, Investigation, Conceptualization.

Declaration of competing interest

The authors declare that they have no known competing financial interests or personal relationships that could have appeared to influence the work reported in this paper.

Acknowledgments

Funding

This work was funded by the Nederlandse Organisatie voor Wetenschappelijk Onderzoek (NWO), Veni grant VI.Veni.222.332 (WKL), NESSC Gravitation Grant 024.002.001 (CPS), Dutch National Science Foundation grant NWO ALWOP.19 (FJH, PRDM, MLL), ERC Marix grant 854088 (CPS). Dr. Schurmannfonds grant 126–2017 (FJH, PRDM, MLL).

Appendix A. Supplementary data

Supplementary material related to this article can be found online at https://doi.org/10.1016/j.chemgeo.2025.122857.

Data availability

All data used in this study is published before. The model code and associated data are included in the submission.

References

Alcott, L.J., Mills, B.J., Bekker, A., Poulton, S.W., 2022. Earth's Great Oxidation Event facilitated by the rise of sedimentary phosphorus recycling. Nat. Geosci. 15, 210–215. http://dx.doi.org/10.1038/s41561-022-00906-5.

Anbar, A.D., Buick, R., Gordon, G.W., Johnson, A.C., Kendall, B., Lyons, T.W., Ostrander, C.M., Planavsky, N.J., Reinhard, C.T., Stüeken, E.E., 2023. Technical comment on "Reexamination of 2.5-Ga 'whiff'of oxygen interval points to anoxic ocean before GOE". Sci. Adv. 9, eabq3736.

Anbar, A.D., Duan, Y., Lyons, T.W., Arnold, G.L., Kendall, B., Creaser, R.A., Kaufman, A.J., Gordon, G.W., Scott, C., Garvin, J., Buick, R., 2007. A whiff of oxygen before the great oxidation event? Science 317, 1903–1906. http://dx.doi.org/10.1126/science.1140325.

Beal, E.J., House, C.H., Orphan, V.J., 2009. Manganese- and iron-dependent marine methane oxidation. Science 325, 184–187. http://dx.doi.org/10.1126/science.1169984.

Bjerrum, C.J., Canfield, D.E., 2002. Ocean productivity before about 1.9 Gyr ago limited by phosphorus adsorption onto iron oxides. Nature 417, 159–162. http://dx.doi.org/10.1038/417159a.

Boudreau, B.P., 1997. Diagenetic models and their implementation. Modelling transport and reactions in aquatic sediments. 505, 436. http://dx.doi.org/10.1007/97S-3-642-60421-S.

Canfield, D.E., 2005. The early history of atmospheric oxygen: Homage to robert m. Garrels. Annu. Rev. Earth Planet. Sci. 33, 1–36. http://dx.doi.org/10.1146/annurev.earth.33.092203.122711.

Canfield, D.E., Rosing, M.T., Bjerrum, C., 2006. Early anaerobic metabolisms. In: Philosophical Transactions of the Royal Society B: Biological Sciences. pp. 1819–1836. http://dx.doi.org/10.1098/rstb.2006.1906.

Cappellen, P.V., Wang, Y., 1996. Cycling of iron and manganese in surface sediments: A general theory for the coupled transport and reaction of carbon, oxygen, nitrogen, sulfur, iron, and manganese. Am. J. Sci. 296, 197–243. http://dx.doi.org/10.2475/ajs.296.3.197.

Catling, D.C., Zahnle, K.J., McKay, C.P., 2001. Biogenic methane, hydrogen escape, and the irreversible oxidation of early earth. Science 293, 839–843. http://dx.doi.org/10.1126/science.1061976.

Chan, C.S., Emerson, D., Luther, III, G.W., 2016. The role of microaerophilic Fe-oxidizing micro-organisms in producing banded iron formations. Geobiology 14, 509–528.

Cohen, P.A., Kodner, R.B., 2022. The earliest history of eukaryotic life: uncovering an evolutionary story through the integration of biological and geological data. Trends Ecol. Evolut. 37, 246–256.

Crockford, P., Halevy, I., 2022. Questioning the paradigm of a phosphate-limited archean biosphere. Geophys. Res. Lett. 49, e2022GL099818.

Crowe, S.A., Katsev, S., Leslie, K., Sturm, A., Magen, C., Nomosatryo, S., Pack, M.A., Kessler, J.D., Reeburgh, W.S., Roberts, J.A., González, L., Haffner, G.D., Mucci, A., Sundby, B., Fowle, D.A., 2011. The methane cycle in ferruginous Lake Matano. Geobiology 9, 61–78. http://dx.doi.org/10.1111/j.1472-4669.2010.00257.x.

Crowe, S.A., Paris, G., Katsev, S., Jones, C.A., Kim, S.T., Zerkle, A.L., Nomosatryo, S., Fowle, D.A., Adkins, J.F., Sessions, A.L., Farquhar, J., Canfield, D.E., 2014. Sulfate was a trace constituent of Archean seawater. Science 346, 735–739. http://dx.doi.org/10.1126/science.1258966.

Derry, L.A., 2015. Causes and consequences of mid-proterozoic anoxia. Geophys. Res. Lett. 42, 8538–8546. http://dx.doi.org/10.1002/2015GL065333.

Egger, M., Rasigraf, O., Sapart, C.J., Jilbert, T., Jetten, M.S., Röckmann, T., Veen, C.V.D., Bânda, N., Kartal, B., Ettwig, K.F., Slomp, C.P., 2015. Iron-mediated anaerobic oxidation of methane in brackish coastal sediments. Environ. Sci. Technol. 49, 277–283. http://dx.doi.org/10.1021/es503663z.

Filippelli, G.M., 2011. Phosphate rock formation and marine phosphorus geochemistry: The deep time perspective. Chemosphere 84, 759–766. http://dx.doi.org/10.1016/j.chemosphere.2011.02.019.

Fournier, G.P., Moore, K.R., Rangel, L.T., Payette, J.G., Momper, L., Bosak, T., 2021. The Archean origin of oxygenic photosynthesis and extant cyanobacterial lineages. Proc. R. Soc. B 288, 20210675.

Habicht, K.S., Gade, M., Thamdrup, B., Berg, P., Canfield, D.E., 2002. Calibration of sulfate levels in the Archean ocean. Science 298, 2372–2374. http://dx.doi.org/10.1126/science.1078265.

Halevy, I., Alesker, M., Schuster, E.M., Popovitz-Biro, R., Feldman, Y., 2017. A key role for green rust in the Precambrian oceans and the genesis of iron formations. Nat. Geosci. 10, 135–139. http://dx.doi.org/10.1038/ngeo2878.

Hao, J., Knoll, A.H., Huang, F., Hazen, R.M., Daniel, I., 2020a. Cycling phosphorus on the Archean earth: Part I. Continental weathering and riverine transport of phosphorus. Geochim. Cosmochim. Acta 273, 70–84. http://dx.doi.org/10.1016/j.gca.2020.01.027.

Hao, J., Knoll, A.H., Huang, F., Schieber, J., Hazen, R.M., Daniel, I., 2020b. Cycling phosphorus on the Archean earth: Part II. Phosphorus limitation on primary production in Archean ecosystems. Geochim. Cosmochim. Acta 280, 360–377. http://dx.doi.org/10.1016/j.gca.2020.04.005.

Holland, H.D., 2006. The oxygenation of the atmosphere and oceans. Phil. Trans. R. Soc. B 361, 903–915. http://dx.doi.org/10.1098/rstb.2006.1838.

Jones, C., Nomosatryo, S., Crowe, S.A., Bjerrum, C.J., Canfield, D.E., 2015. Iron oxides, divalent cations, silica, and the early earth phosphorus crisis. Geology 43, 135–138. http://dx.doi.org/10.1130/G36044.1.

Kappler, A., Pasquero, C., Konhauser, K.O., Newman, D.K., 2005. Deposition of banded iron formations by anoxygenic phototrophic Fe(II)-oxidizing bacteriaa. Geology 33, 865–868. http://dx.doi.org/10.1130/G21658.1.

Kendall, B., Reinhard, C.T., Lyons, T.W., Kaufman, A.J., Poulton, S.W., Anbar, A.D., 2010. Pervasive oxygenation along late archaean ocean margins. Nat. Geosci. 3, 647–652.

Kipp, M.A., Stüeken, E.E., 2017. Biomass recycling and earth's early phosphorus cycle. Sci. Adv. 3, 1–7. http://dx.doi.org/10.1126/sciadv.aao4795.

Konhauser, K.O., Hamade, T., Raiswell, R., Morris, R.C., Ferris, F.G., Southam, G., Canfield, D.E., 2002. Could bacteria have formed the Precambrian banded iron formations? Geology 30, 1079–1082.

Konhauser, K.O., Newman, D.K., Kappler, A., 2005. The potential significance of microbial Fe (III) reduction during deposition of Precambrian banded iron formations. Geobiology 3, 167–177.

Konhauser, K.O., Planavsky, N.J., Hardisty, D.S., Robbins, L.J., Warchola, T.J., Haugaard, R., Lalonde, S.V., Partin, C.A., Oonk, P.B., Tsikos, H., Lyons, T.W., Bekker, A., Johnson, C.M., 2017. Iron formations: A global record of neoarchaean to palaeoproterozoic environmental history. Earth-Sci. Rev. 172, 140–177. http://dx.doi.org/10.1016/j.earscirev.2017.06.012.

Lantink, M.L., Davies, J.H.F.L., Ovtcharova, M., Hilgen, F.J., 2022. Milankovitch cycles in banded iron formations constrain the Earth–Moon system 2.46 billion years ago. Proc. Natl. Acad. Sci. 119, e2117146119.

Lantink, M.L., Lenstra, W.K., Davies, J.H.F.L., Hennekam, R., Mcb, D., Mason, P.R.D., jan Reichart, G., Slomp, C.P., Hilgen, F.J., 2023. Precessional pacing of early proterozoic redox cycles. Earth Planet. Sci. Lett. 610, 118117. http://dx.doi.org/10.1016/j.epsl.2023.118117.

Lenstra, W.K., van Helmond, N.A., Martins, P.D., Wallenius, A.J., Jetten, M.S., Slomp, C.P., 2023. Gene-based modeling of methane oxidation in coastal sediments: Constraints on the efficiency of the microbial methane filter. Environ. Sci. Technol. 57, 12722–12731. http://dx.doi.org/10.1021/acs.est.3c02023.

Lyons, T.W., Reinhard, C.T., Planavsky, N.J., 2014. The rise of oxygen in Earth's early ocean and atmosphere. Nature 506, 307–315. http://dx.doi.org/10.1038/nature13068.

Millero, F.J., Sotolongo, S., Izaguirre, M., 1987. The oxidation kinetics of Fe(II) in seawater. Geochim. Cosmochim. Acta 51, 793–801. http://dx.doi.org/10.1016/0016-7037(87)90093-7.

Olson, S.L., Reinhard, C.T., Lyons, T.W., 2016. Limited role for methane in the mid-Proterozoic greenhouse. Proc. Natl. Acad. Sci. USA 113, 11447–11452. http://dx.doi.org/10.1073/pnas.1608549113.

Ostrander, C.M., Johnson, A.C., Anbar, A.D., 2021. Earth's first redox revolution. Annu. Rev. Earth Planet. Sci. 49, 337–366.

Poulton, S.W., Bekker, A., Cumming, V.M., Zerkle, A.L., Canfield, D.E., Johnston, D.T., 2021. A 200-million-year delay in permanent atmospheric oxygenation. Nature 592, 232–236. http://dx.doi.org/10.1038/s41586-021-03393-7.

Reinhard, C.T., Planavsky, N.J., Gill, B.C., Ozaki, K., Robbins, L.J., Lyons, T.W., Fischer, W.W., Wang, C., Cole, D.B., Konhauser, K.O., 2017. Evolution of the global phosphorus cycle. Nature 541, 386–389. http://dx.doi.org/10.1038/nature20772.

Ruttenberg, K.C., 2013. The global phosphorus cycle. In: Treatise on Geochemistry: Second Edition. 10, pp. 499–558. http://dx.doi.org/10.1016/B978-0-08-095975-7.00813-5.

Steinsdóttir, H.G.R., Schauberger, C., Mhatre, S., Thamdrup, B., Bristow, L.A., 2022. Aerobic and anaerobic methane oxidation in a seasonally anoxic basin. Limnol. Oceanogr. 67, 1257–1273. http://dx.doi.org/10.1002/lno.12074.

Thompson, K.J., Kenward, P.A., Bauer, K.W., Warchola, T., Gauger, T., Martinez, R., Simister, R.L., Michiels, C.C., Llirós, M., Reinhard, C.T., Kappler, A., Konhauser, K.O., Crowe, S.A., 2019. Photoferrotrophy, deposition of banded iron formations, and methane production in Archean oceans. Sci. Adv. 5, 1–10. http://dx.doi.org/10.1126/sciadv.aav2869.

Trendall, A.F., Blockley, J.G., 1968. Stratigraphy of the dales gorge member of the Brockman iron formation in the precambrian hamersley group of western Australia. Geol. Surv. West. Aust. Annu. Rep. for 1967, 48–53.

Venetz, J., Żygadłowska, O.M., Dotsios, N., Wallenius, A.J., van Helmond, N.A.G.M., Lenstra, W.K., Klomp, R., Slomp, C.P., Jetten, M.S.M., Veraart, A.J., 2024. Seasonal dynamics of the microbial methane filter in the water column of a eutrophic coastal basin. FEMS Microbiol. Ecol. 100, fiae007. http://dx.doi.org/10.1093/femsec/fiae007.

Walton, C.R., Ewens, S., Coates, J.D., Blake, R.E., Planavsky, N.J., Reinhard, C., Ju, P., Hao, J., Pasek, M.A., 2023. Phosphorus availability on the early Earth and the impacts of life. Nat. Geosci. 16, 399–409. http://dx.doi.org/10.1038/s41561-023-01167-6.

Wang, Y.F., Cappellen, P.V., 1996. A multicomponent reactive transport model of early diagenesis: Application to redox cycling in coastal marine sediments. Geochim. Cosmochim. Acta 60, 2993–3014. http://dx.doi.org/10.1016/0016-7037(96)00140-8.

Widdel, F., Schnell, S., Heising, S., Ehrenreich, A., Assmus, B., Schink, B., 1993. Ferrous iron oxidation by anoxygenic phototrophic bacteria. Nature 362, 834–836.

Wogan, N.F., Catling, D.C., Zahnle, K.J., Claire, M.W., 2022. Rapid timescale for an oxic transition during the Great Oxidation Event and the instability of low atmospheric O2. Proc. Natl. Acad. Sci. 119, e2205618119.

Zhelezinskaia, I., Kaufman, A.J., Farquhar, J., Cliff, J., 2014. Large sulfur isotope fractionations associated with Neoarchean microbial sulfate reduction. Science 346, 742–744. http://dx.doi.org/10.1126/science.1256211.

Żygadłowska, O.M., Roth, F., van Helmond, N.A., Lenstra, W.K., Venetz, J., Dotsios, N., Röckmann, T., Veraart, A.J., Stranne, C., Humborg, C., Jetten, M.S., Slomp, C.P., 2024a. Eutrophication and deoxygenation drive high methane emissions from a Brackish Coastal system. Environ. Sci. Technol. 58, 10582–10590. http://dx.doi.org/10.1021/acs.est.4c00702.

Żygadłowska, O.M., Venetz, J., Lenstra, W.K., van Helmond, N.A., Klomp, R., Röckmann, T., Veraart, A.J., Jetten, M.S., Slomp, C.P., 2024b. Ebullition drives high methane emissions from a eutrophic coastal basin. Geochim. Cosmochim. Acta 384, 1–13. http://dx.doi.org/10.1016/j.gca.2024.08.028.